Characterization of interface states in Al2O3/AlGaN/GaN structures for improved performance of high-electron-mobility transistors

Y. Hori, Z. Yatabe, and T. Hashizume

Citation: Journal of Applied Physics **114**, 244503 (2013); doi: 10.1063/1.4859576
View online: http://dx.doi.org/10.1063/1.4859576
View Table of Contents: http://scitation.aip.org/content/aip/journal/jap/114/24?ver=pdfcov
Published by the AIP Publishing

Characterization of interface states in Al_2O_3/AlGaN/GaN structures for improved performance of high-electron-mobility transistors

Y. Hori,[1] Z. Yatabe,[1] and T. Hashizume[1,2,a)]
[1]*Research Center for Integrated Quantum Electronics (RCIQE) and Graduate School of Information Science and Technology, Hokkaido University, North 13 West 8, Sapporo, 060-8628 Hokkaido, Japan*
[2]*Japan Science and Technology Agency (JST), CREST, Tokyo 102-0075, Japan*

(Received 11 November 2013; accepted 14 December 2013; published online 27 December 2013)

We have investigated the relationship between improved electrical properties of Al_2O_3/AlGaN/GaN metal-oxide-semiconductor high-electron-mobility transistors (MOS-HEMTs) and electronic state densities at the Al_2O_3/AlGaN interface evaluated from the same structures as the MOS-HEMTs. To evaluate Al_2O_3/AlGaN interface state densities of the MOS-HEMTs, two types of capacitance-voltage (*C-V*) measurement techniques were employed: the photo-assisted *C-V* measurement for the near-midgap states and the frequency dependent *C-V* characteristics for the states near the conduction-band edge. To reduce the interface states, an N_2O-radical treatment was applied to the AlGaN surface just prior to the deposition of the Al_2O_3 insulator. As compared to the sample without the treatment, the N_2O-radical treated Al_2O_3/AlGaN/GaN structure showed smaller frequency dispersion of the *C-V* curves in the positive gate bias range. The state densities at the Al_2O_3/AlGaN interface were estimated to be $1 \times 10^{12}\,cm^{-2}\,eV^{-1}$ or less around the midgap and $8 \times 10^{12}\,cm^{-2}\,eV^{-1}$ near the conduction-band edge. In addition, we observed higher maximum drain current at the positive gate bias and suppressed threshold voltage instability under the negative gate bias stress even at 150 °C. Results presented in this paper indicated that the N_2O-radical treatment is effective both in reducing the interface states and improving the electrical properties of the Al_2O_3/AlGaN/GaN MOS-HEMTs. © *2013 AIP Publishing LLC*. [http://dx.doi.org/10.1063/1.4859576]

I. INTRODUCTION

GaN and related-material high-electron-mobility transistors (HEMTs) are promising for high-power and high-frequency device applications, owing to their good physical properties such as high-breakdown electric field and high-saturation electron velocity.[1] In particular, high-density and high-mobility two dimensional electron gas (2DEG) generated at the AlGaN/GaN interface enables us to realize power switching transistors having extremely low on-state resistance applicable to next generation power conversion systems.[2–5] To achieve normally-off operation, metal-oxide-semiconductor (MOS) gate structures are absolutely required for suppressing gate leakage current under a forward gate bias operation. For realizing a good insulated gate, we should consider material properties of insulators: wide bandgap leading to large band offset against GaN-based-materials, high breakdown field, and high permittivity. In addition, low-density electronic states at the insulator/GaN-based-material interfaces are also necessary because interface states may cause various operational stability and reliability issues in GaN-based MOS-HEMTs such as threshold voltage instability and current collapse phenomenon. To address these issues, it is essential to investigate not only the densities of electronic states at the insulator/GaN-based-material interfaces but also the various process conditions to control them.

Al_2O_3 is one of the leading candidates for gate insulators in GaN-based devices. GaN-based MOS-HEMTs using an Al_2O_3 as the insulator have been demonstrated by many groups.[3,4,6–9] The typical values of bandgap and permittivity reported for the Al_2O_3 film are 7–9 eV and 8–10, respectively.[6–10] The Al_2O_3 film prepared by atomic layer deposition (ALD), in particular, showed relatively low electronic state densities in the Al_2O_3/n-GaN system.[9,11–13] However, in the MOS-HEMT structures, the insulator/semiconductor interface is usually formed on the AlGaN/GaN heterostructures, resulting in the existence of two interfaces under the gate electrode. In this case, because those two interfaces make potential control rather complicated during capacitance-voltage (*C-V*) measurements, it is difficult to characterize interface states in the MOS-HEMTs compared with MOS structures having a single semiconductor layer (e.g., the Al_2O_3/n-GaN structure). Moreover, the wide bandgap of GaN-based materials also leads to extremely low emission rate of electrons captured at the interface states, making the evaluation of interface state densities difficult. For example, a typically used AlGaN with an Al composition ratio of around 25% has a bandgap of approximately 4.0 eV. Accordingly, the time constant for thermal electron emission from its midgap (~2.0 eV) is estimated to be several years at room temperature. It means that only a limited number of the interface states can be detected during the standard *C-V* measurements. Although several groups have proposed new methods to characterize electronic states in the MOS-HEMT structures,[14–17] there have been few reports on MOS interface state densities of the GaN-based MOS-HEMTs and their relationship to the resulting electrical properties has not been discussed in detail.

In this paper, we have attempted to determine interface state density distributions of Al_2O_3/AlGaN/GaN MOS-HEMTs using two types of *C-V* analysis, the photo-assisted

a)Electronic mail: hashi@rciqe.hokudai.ac.jp

measurement and the frequency dispersion characterization. We then discuss the relationship between the interface states and resulting electrical properties including threshold voltage instability of the MOS-HEMTs.

II. FABRICATION PROCESS

Figure 1 schematically shows the structure of the fabricated Al_2O_3/AlGaN/GaN MOS-HEMT. We used an $Al_{0.23}Ga_{0.77}N$/GaN heterostructure grown on a sapphire substrate by metal organic chemical vapor deposition. Sheet resistance and electron mobility of the heterostructure were estimated to be 440 Ω/sq and 1770 cm^2/Vs, respectively. In this study, we employed the "ohmic-first" process to prevent damage to the Al_2O_3 film during ohmic annealing.[11] After the pretreatment of the sample surface in a 30%-HF solution for 5 min, we deposited a 10 nm SiN as a surface protection layer by electron cyclotron resonance chemical vapor deposition. Ti/Al/Ti/Au (=20/50/20/100 nm) source and drain electrodes were then deposited on the AlGaN surface, followed by ohmic annealing at 800 °C for 1 min in N_2 ambient. Device isolation was performed in a reactive ion beam etching chamber using CH_4-based plasma. After removing the SiN layer with a buffered HF, we applied an N_2O-radical treatment to the AlGaN surface.[18] A 10-nm-thick Al_2O_3 gate insulator was then deposited at 350 °C by ALD (SUGA-SAL1500) using trimethylaluminum and water vapor as precursors. To improve the interface properties, we also performed post deposition annealing at 450 °C for 15 min in N_2 ambient. Finally, a Ni/Au (=20/50 nm) gate electrode was deposited on the Al_2O_3 layer. Gate length and width of the MOS-HEMTs were 3 and 100 μm, respectively. For *C-V* characterization, we also fabricated Al_2O_3/AlGaN/GaN diode structures having circular gate and ring-shaped ohmic electrodes on the same chip.

III. EXPERIMENT

A. Typical *C-V* characteristics of Al_2O_3/AlGaN/GaN diode structures

Figure 2 shows the *C-V* characteristics of the Al_2O_3/AlGaN/GaN diode structures without and with the N_2O-radical treatment prepared on the same chip as the MOS-HEMTs. We carried out *C-V* measurements using Agilent 4294A Precision Impedance Analyzer. The gate bias

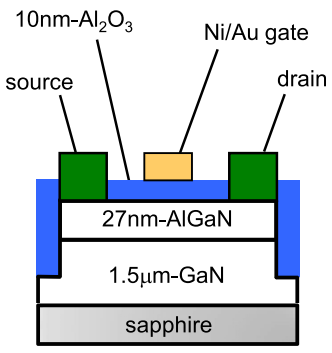

FIG. 1. Schematic cross-sectional view of the Al_2O_3/AlGaN/GaN MOS-HEMT structure.

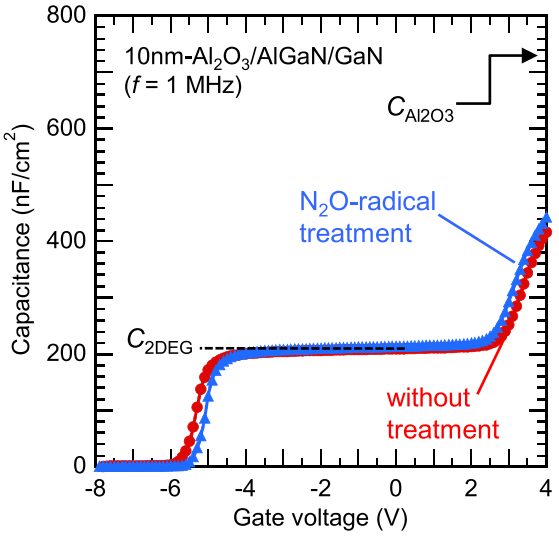

FIG. 2. *C-V* characteristics of the Al_2O_3/AlGaN/GaN MOS diode structures without and with the N_2O-radical treatment.

was swept from +4 to −8 V with a 0.05 V-step. The sweep rate was approximately 300 ms/step. The measurement frequency was 1 MHz. For both samples without and with the N_2O-radical treatment, we obtained peculiar *C-V* curves having a two-step capacitance change, which is the characteristic feature of the MOS-HEMT structure having two interfaces.[14] The nearly flat capacitance C_{2DEG} around zero bias indicates that the 2DEG accumulates at the AlGaN/GaN interface. When we apply the positive gate bias, electrons start to distribute in the AlGaN layer, leading to the increase of capacitance to the insulator capacitance C_{Al2O3}. Because the maximum gate bias was limited to +4 V by the gate leakage current, C_{Al2O3} corresponding to the 10-nm-thick Al_2O_3 was not observed here. However, C_{2DEG} around the zero bias is in accordance with the series capacitance of the 10-nm-thick Al_2O_3 and the 27-nm-thick AlGaN. When the gate bias nears the threshold voltage (V_{th}) in the negative bias range, the depletion of the 2DEG leads to the steep decrease of capacitance, corresponding to the 2nd *C-V* step.

B. Effect of MOS interface states in *C-V* measurements

To understand basic behavior of interface states in the *C-V* curves of the MOS-HEMT structures, we calculated the *C-V* characteristics of the MOS-HEMTs using a numerical solver of the one-dimensional Poisson equation designed by Miczek *et al.*[19] In the calculation, we assumed the high-frequency limit in which all the interface states cannot respond to the ac signal but only follow the dc gate bias change. As indicated by the solid line in Fig. 3(a), the ideal *C-V* curve shows a two-step capacitance change which is also observed in the experimental data. C_{2DEG} is also in agreement with those in Fig. 2. The two broken lines show an example of the *C-V* calculation assuming the two typical interface state density D_{it} distributions, D_{it1} and D_{it2} ($>D_{it1}$), shown in Fig. 3(b). In the D_{it} distributions, the charge neutrality level E_{CNL} is a branch point for acceptor- and donor-like interface states having a U-shaped distribution

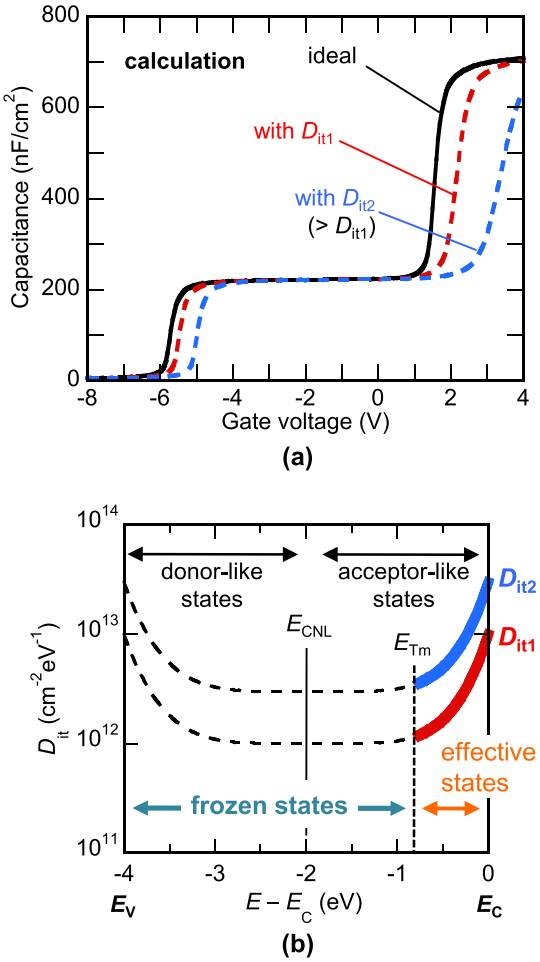

FIG. 3. (a) Calculated *C-V* characteristics of the Al_2O_3/AlGaN/GaN structures. (b) Al_2O_3/AlGaN interface density distributions assumed in the calculation.

which is in accordance with the disorder-induced gap state model. Additionally, we also took into account time constants for electron emission from the interface states using the Shockley-Read-Hall (SRH) statistics. In Fig. 3(b), E_{Tm} is the deepest energy of the state which can respond during the actual *C-V* sweeping time t_{meas}. E_{Tm} can be described by using SRH statistics as follows:

$$E_{Tm} = kT\ln(\sigma N_C \upsilon t_{meas}), \tag{1}$$

where k, T, and σ are the Boltzmann constant, temperature, and the capture cross section of the interface states, and N_C and υ are the effective density of states in the conduction band of the AlGaN and the thermal velocity of electrons, respectively. Assuming that σ is 1×10^{-16} cm^2 and t_{meas} is 100 s, E_{Tm} was estimated to be 0.8 eV from the conduction-band edge in the Al_2O_3/AlGaN system. It means, therefore, that only 25% or less of the interface states can be detected while the others are in "frozen states" which cannot de-trap electrons during the *C-V* sweeping at room temperature. As shown in Fig. 3(a), the interface states led to on-set voltage shifts toward the positive direction and stretch-out of *C-V* curves in the positive bias range. This is due to the change of the interface state charge within the "effective states" when the Fermi level E_F is moving between the conduction-band edge E_C and E_{Tm}. In the negative bias range, in contrast, only parallel voltage shifts were observed. When E_F moves down toward the valence-band edge E_V at the Al_2O_3/AlGaN interface, the "frozen states" in the energy range of E_{Tm} to E_V cannot change their electron occupation rate because their corresponding time constants are longer than the sweeping time of 100 s. Because the interface charge density is not a function of the gate bias during the negative bias sweep, the interface states do not cause the stretch-out behavior. It follows, therefore, that the detection of the interface states using the standard *C-V* technique in the negative bias region is difficult.

For the sample subjected to the N_2O-radical treatment, as shown in Fig. 2, the smaller on-set voltage in the positive bias region probably indicates the reduction of the Al_2O_3/AlGaN interface states. However, the slopes of both *C-V* curves were not so different from each other. In the MOS-AlGaN/GaN systems, it is rather difficult to apply Terman method[20] to the interface state characterization, because we cannot determine one surface potential in the MOS-HEMT structures having two interfaces from one gate capacitance value. Fagerlind *et al.*[21] utilized the frequency dispersion characteristics of the *C-V* curves in the positive bias range for estimating interface state densities. They evaluated the MIS interface state densities near the conduction-band edge for SiN/AlGaN/AlN/GaN structures. Mizue *et al.*[14] developed the photo-assisted *C-V* measurement using monochromatic lights with photon energies less than the bandgap of the AlGaN. They analyzed photo-induced V_{th} shifts in the negative bias range and reported the MOS interface state densities around the midgap of the Al_2O_3/AlGaN/GaN structure for the first time. In this paper, we have employed the combination of those techniques, the frequency dispersion method and the photo-assisted measurement, for the characterization of the Al_2O_3/AlGaN interface states of the MOS-HEMTs.

C. Frequency dispersion *C-V* characteristics

Figure 4 compares the frequency dispersion of the *C-V* characteristics of the MOS-HEMTs without and with the N_2O-radical treatment. The measurement frequencies were 1 kHz, 10 kHz, 100 kHz, and 1 MHz. In the positive bias range, we clearly observed frequency dispersion for the both samples probably caused by electron capture and emission at the Al_2O_3/AlGaN interface states. For the N_2O-radical treated sample, in particular, the smaller dispersion between those frequencies indicates the reduction of interface states. The relationship between the time constant τ_1 and the frequency f_1 is given by Eq. (2)

$$\tau_1 = \frac{1}{2\pi f_1}, \tag{2}$$

and the trap energy depth E_1 corresponding to f_1 is expressed by the SRH statistics as follows:

$$E_1 = kT\ln\left(\frac{\sigma N_C \upsilon}{2\pi f_1}\right). \tag{3}$$

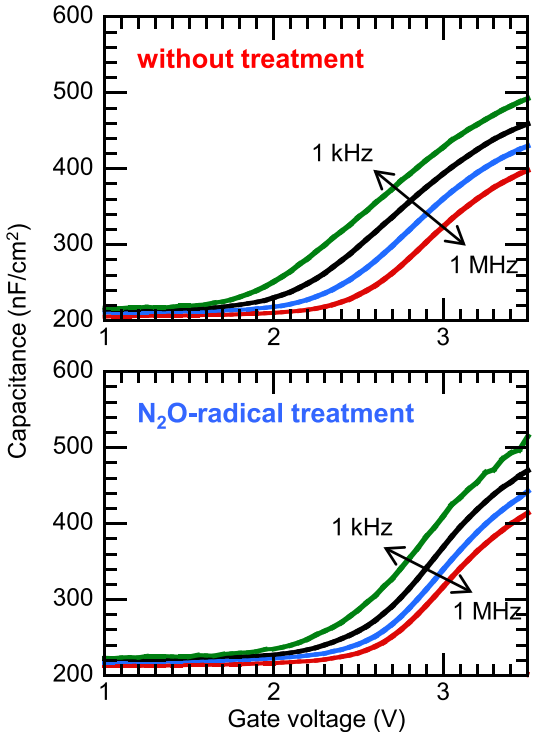

FIG. 4. Frequency dispersion of the C-V characteristics of the Al_2O_3/AlGaN/GaN MOS diode structures without and with the N_2O-radical treatment in the positive bias range.

As schematically shown in Fig. 5, the interface states distributed within the bandgap can be divided into two parts by E_1. In the upper energy range which has faster time constants than the measurement frequency ($\tau < 1/2\pi f_1$), electron capture and emission at the interface states can respond to the ac gate signal. In this case, the interface trap capacitance C_{it} and resistance R_{it} associated with electron capture and emission at the interface states are connected parallel to the depletion capacitance (the AlGaN capacitance C_{AlGaN}, in this case).[22] Consequently, that leads to the overestimation of the measurement capacitance when the Fermi level is located in the energy range of E_C to E_1. In the lower energy range which has longer time constants ($\tau > 1/2\pi f_1$), on the other hand, the C_{it} and R_{it} can be ignored because the

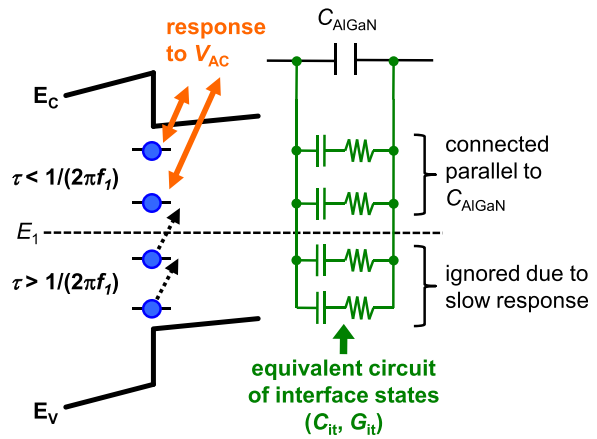

FIG. 5. Equivalent circuit of the interface states in Al_2O_3/AlGaN/GaN structures during the C-V measurement.

interface states do not respond to the ac signal. Using a lower frequency f_2, the trap energy depth E_2 at which C_{it} starts to be detected becomes deeper. This leads to the overestimation of the capacitance at the smaller gate bias, causing a leftward on-set voltage shift for the lower frequencies in the positive bias region. Note that such overestimation of the capacitance increasing with D_{it} is not observed in the C-V calculation shown in Fig. 3(a) because the present calculation does not take into account the frequency response of the interface states. To estimate D_{it} from the experimental data, we then focused on the on-set voltage shifts in the frequency dependent C-V curves.

Fig. 6(a) compares the C-V characteristics of the sample without the treatment measured at 100 kHz and 1 MHz in the positive bias range. The on-set voltage difference ΔV between two frequencies (f_1, f_2) corresponds to the interface charge density ΔQ_{it} in the energy range of E_1 to E_2 as schematically shown in Fig. 6(b). E_1 and E_2 were estimated to be 0.17 and 0.23 eV, respectively, using Eq. (3), where f_1, f_2, and σ are 1 MHz, 100 kHz and 1×10^{-16} cm^2, respectively. In this energy range, D_{it} can be estimated from the following equation:

$$D_{it}(E = E_{AVG}) = \frac{C_{Al2O3}}{q}\frac{|V_2 - V_1|}{E_2 - E_1} = \frac{C_{Al2O3}}{q}\frac{\Delta V}{\Delta E}, \quad (4)$$

where V_1 and V_2 are the on-set voltages for f_1 and f_2, respectively.[21] E_{AVG} is the average energy between E_1 and E_2, as described by Eq. (5)

$$E_{AVG} = E_1 + \frac{E_2 - E_1}{2} = E_1 + \Delta E/2. \quad (5)$$

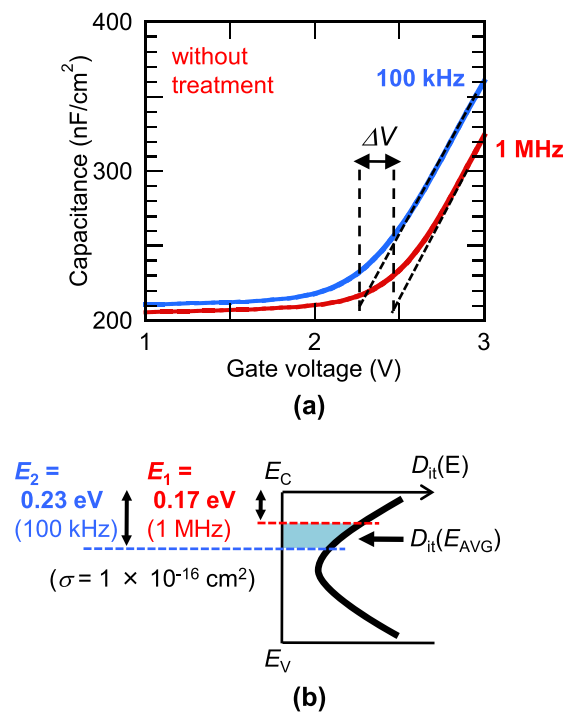

FIG. 6. (a) C-V curves of the sample without the surface treatment measured at frequencies of 100 kHz and 1 MHz. (b) Schematic illustration of D_{it} energy ranges corresponding to measurement frequencies.

Although we have to assume a value of σ in E_1 (as suggested in Eq. (3)) to determine the energy position of D_{it}, the energy difference ΔE, which is also used in Eq. (4), is independent of σ but dependent on T, f_1, and f_2, as described by Eq. (6)

$$\Delta E = E_2 - E_1 = kT\ln\left(\frac{\sigma N_C \upsilon}{2\pi f_2}\right) - kT\ln\left(\frac{\sigma N_C \upsilon}{2\pi f_1}\right) = kT\ln(f_1/f_2). \tag{6}$$

Therefore, D_{it} can be evaluated using Eq. (4) without assuming a value of σ. Supposing that σ is constant for both samples without and with the N_2O-radical treatment, we can compare the D_{it} distributions of both samples in the same energy range.

IV. RESULTS AND DISCUSSION

A. Estimate of D_{it} in Al_2O_3/AlGaN/GaN MOS-HEMTs

Figure 7 shows the results of the D_{it} distributions at the Al_2O_3/AlGaN interface in the MOS-HEMT structures estimated using the combination of the frequency dispersion C-V method and the photo-assisted C-V measurement. In the frequency dispersion method, we assumed σ to be $1 \times 10^{-16}\,cm^2$, giving values of D_{it} in the energy range of -0.2 to -0.32 eV from E_C. For the sample without the treatment, D_{it} near the conduction-band edge was estimated to be $2\text{–}3 \times 10^{13}\,cm^{-2}\,eV^{-1}$, which is about one order higher than those reported for the Al_2O_3/n-GaN system.[11] As Ooyama *et al.* reported in Ref. 23, the defect level densities of AlGaN were about 10 times as high as those of GaN, probably due to high densities of defects related to nitrogen vacancy, oxygen impurity, and their complexes.[24] It is likely that they also led to the higher densities of interface states in Al_2O_3/AlGaN compared with those in the Al_2O_3/n-GaN system. We also carried out the photo-assisted C-V measurement using monochromatic lights with photon energies of 1.4–2.2 eV.[18] For the sample without the surface treatment, the minimum state densities around the midgap were estimated to be around $2 \times 10^{12}\,cm^{-2}\,eV^{-1}$, which is in good agreement with the data reported for the Al_2O_3/AlGaN/GaN structure.[14] As already reported in Ref. 18, in comparison, the N_2O-radical treated sample showed a lower D_{it} distribution around the midgap with a minimum density of less than $1 \times 10^{12}\,cm^{-2}\,eV^{-1}$. Moreover, the state densities near the conduction-band edge were estimated to be $8 \times 10^{12}\,cm^{-2}\,eV^{-1}$ for the N_2O-radical treated Al_2O_3/AlGaN interface. Supposing that the D_{it} distributions of both samples are U-shaped as indicated by the broken lines in Fig. 7, the entire acceptor-like state density distribution of the N_2O-radical treated MOS-HEMT is expected to be reduced by approximately 40% compared with that of the sample without the treatment. Assuming those entire D_{it} distributions to the numerical solver, the calculated C-V curves reasonably reproduced the experimental data for the both samples at 1 MHz (not shown here). For further consideration of the D_{it} estimation, not only the methods presented here but also other approaches to C-V analyses are necessary. However, the present N_2O-radical treatment appears also to be effective in improving the electrical properties of the AlGaN/GaN MOS-HEMTs.

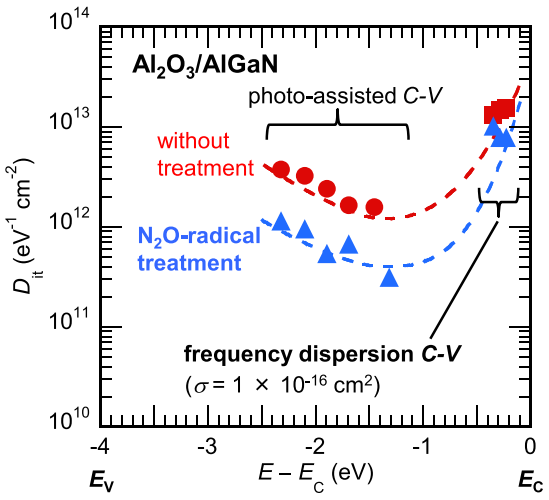

FIG. 7. Al_2O_3/AlGaN interface state density distributions in the Al_2O_3/AlGaN/GaN structures without and with the N_2O-radical treatment.

B. Chemical properties of N_2O-radical treated AlGaN surface

To investigate the chemical bonding properties of the N_2O-radical treated AlGaN surface, we carried out X-ray photoelectron spectroscopy (XPS) analysis using a monochromatic Al Kα radiation source ($h\nu = 1486.6$ eV). Figure 8 compares the O 1s and N 1s core-level spectra of the AlGaN surfaces before and after the N_2O-radical treatment taken with a photoelectron escape angle of 15°. Note that each spectrum was normalized to the Ga 3d peak. As indicated by

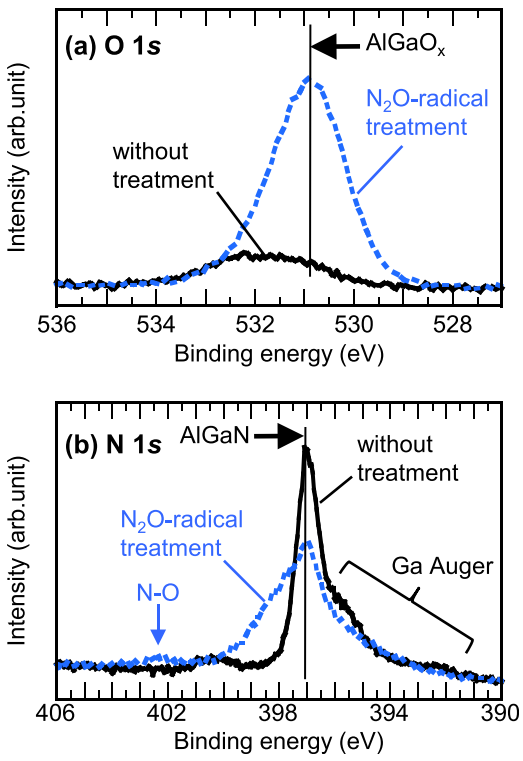

FIG. 8. (a) O 1s and (b) N 1s core-level spectra obtained from the AlGaN surfaces before and after the N_2O-radical treatment.

the broken line in Fig. 8(a), the increase of the $AlGaO_x$ peak was observed for the N_2O-radical treated AlGaN surface, probably arising from the oxidation of the AlGaN due to the treatment.[25,26] We also confirmed chemical shifts in the Ga 3*d* and Al 2*p* core-level spectra (not shown here).[27] In the N 1*s* spectra shown in Fig. 8(b), however, the AlGaN peak at 397.0 eV is decreased for the N_2O-radical treated sample but still remains and overlaps with the broadened Ga *LMM* Auger spectra.[28] The broader linewidth and the chemical shift of Ga Auger signal were also observed in the GaO_x layer prepared by photoelectrochemical oxidation of GaN.[29] That is, the XPS spectra obtained from the N_2O-radical treated surface contain those of the AlGaN and AlGa-oxide layers, suggesting the oxidation layer was very thin (1 nm or less). Bae *et al.*[30] reported that an ultra thin Ga-oxide layer prepared by the remote plasma-assisted oxidation process is effective in reducing interface states for the SiO_2/n-GaN system. Tajima *et al.*[31] compared the oxidation processes for access regions in AlGaN/GaN HEMTs using O_2- and N_2O-plasma treatments. In their report, N_2O plasma promoted the oxidation of the AlGaN surface with an N-O bonding network, which probably suppressed the defect formation in the AlGaN layer during the oxidation process. As shown in Fig. 8(b), we also confirmed the small presence of the N-O bonding peak at around 402.5 eV for the N_2O-radical treated AlGaN surface.[27,31,32] Although the mechanism is not clear yet, it is likely that the monolayer-level formation of the AlGa-oxide layer prepared by the N_2O-radical treatment is effective in reducing electronic states at the Al_2O_3/AlGaN interface.

C. Electrical properties of Al_2O_3/AlGaN/GaN MOS-HEMTs

Figure 9 shows the drain current-voltage (I_{DS}-V_{DS}) characteristics of the Al_2O_3/AlGaN/GaN MOS-HEMTs without and with the N_2O-radical treatment. We used Agilent B1500A Semiconductor Device Analyzer with B1525A High Voltage Semiconductor Pulse Generator Unit for pulsed current-voltage measurements. Pulse width and period were 5 μs and 0.5 s, respectively. The drain-source and gate-source base-voltages were set to 0 V, "no-stress" condition. At the gate-source voltage $V_{GS} = 0$ V, both samples show almost the same current density, indicating no pronounced degradation of the 2DEG channel due to the N_2O-radical treatment. At $V_{GS} = +4$ V, in contrast, the N_2O-radical treated MOS-HEMT shows higher current density than the MOS-HEMT without the treatment. This tendency was also confirmed in the transfer characteristics in the saturation region, as indicated by the solid lines in Fig. 10. For the MOS-HEMT without the treatment, a marked decrease of transconductance was observed at high gate bias range. When the gate bias is positive, electron transfer from the AlGaN/GaN interface to the Al_2O_3/AlGaN interface occurs, which can be confirmed in the *C*-*V* results in Fig. 2, resulting in the parasitic channel formation at the Al_2O_3/AlGaN interface. In this case, the relatively high-density interface states caused the degradation of electron mobility, leading to the decrease of transconductance. In comparison, the improvement of transfer characteristics of the

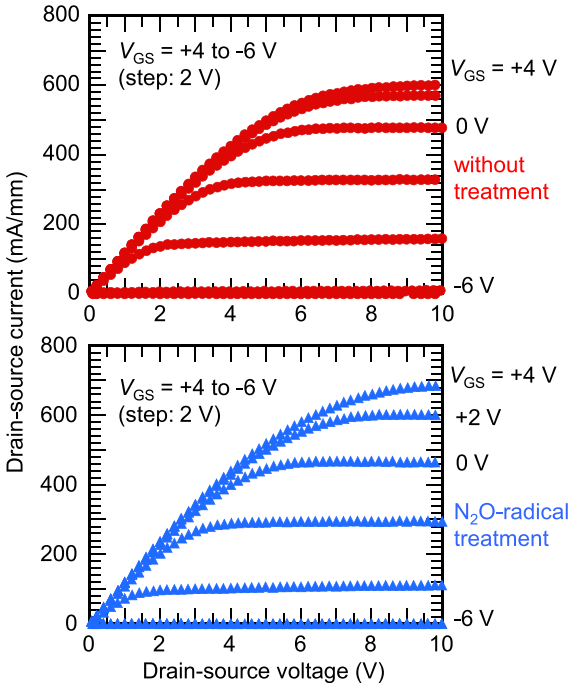

FIG. 9. I_{DS}-V_{DS} characteristics of the Al_2O_3/AlGaN/GaN MOS-HEMTs without and with the N_2O-radical treatment pulsed from "no-stress" bias condition.

N_2O-radical treated MOS-HEMT in the positive gate bias region is due to the reduction of interface states, also as confirmed in Fig. 7.

To investigate the operational stability of the MOS-HEMTs, we also performed negative-gate-bias-induced V_{th} instability measurements. In Fig. 10, the broken lines ("gate-stress") show transfer characteristics pulsed from

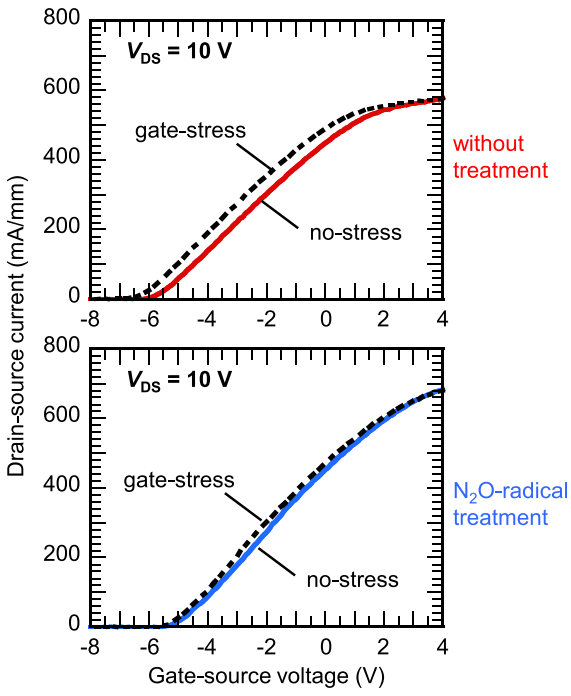

FIG. 10. Transfer characteristics of the Al_2O_3/AlGaN/GaN MOS-HEMTs without and with the N_2O-radical treatment pulsed from "no-stress" (solid lines) and "gate-stress" (broken lines) bias conditions.

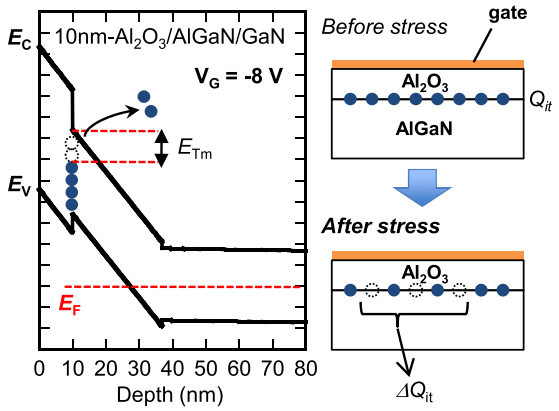

FIG. 11. Calculated potential profile of the Al_2O_3/AlGaN/GaN at $V_{GS} = -8$ V and schematic illustration of the possible mechanism for the negative-gate-bias-induced V_{th} shifts.

negative-gate-bias stress condition, $V_{GS} = -8$ V and $V_{DS} = 0$ V. For the sample without the treatment, we observed a threshold voltage shift ΔV_{th} of 0.7 V toward the negative bias direction, which is probably due to the negative-gate-bias-induced electron emission from the Al_2O_3/AlGaN interface. Figure 11 shows the potential profile of the Al_2O_3/AlGaN/GaN structure calculated by using the numerical Poisson solver. At $V_{GS} = -8$ V, E_F is located far below the valence-band edge at the Al_2O_3/AlGaN interface. In this case, electron at the shallow states which have shorter time constants can be emitted, resulting in the V_{th} shift toward the negative bias direction. Using Eq. (1) and the pulse period of 0.5 s, E_{Tm} for the pulsed measurement can be estimated to be 0.6 eV. When we integrated the expected D_{it} distribution determined in Fig. 7 from E_C to E_{Tm}, the resulting charge density is in good agreement with the charge difference ΔQ_{it} ($=C_{Al2O3}\Delta V_{th}/q$), 3.2×10^{12} cm^{-2}, corresponding to 0.7 V-shift. In contrast, the suppressed V_{th} shift for the N_2O-radical treated MOS-HEMT is clearly due to the reduction of the interface states. For this sample, ΔQ_{it} was estimated to be 1.4×10^{12} cm^{-2} with ΔV_{th} of 0.3 V, which is approximately 40%-less compared with that of the MOS-HEMT without the treatment.

Figure 12 shows the results on the negative-gate-bias-induced V_{th} shifts of the MOS-HEMTs measured at room temperature (RT), 100 °C, and 150 °C. For both samples, the amount of V_{th} shifts increased with increasing temperature. Because E_{Tm} is proportional to the temperature as described in Eq. (1), the larger amount of electron emission caused larger V_{th} shifts toward the negative bias direction. For the N_2O-radical treated MOS-HEMT, however, we observed the smaller V_{th} shift of less than 0.5 V even at 150 °C. The N_2O-radical treated MOS-HEMT shows more stable V_{th} under negative-gate bias stress at high temperatures due to the reduction of interface states. The results presented in this paper are the first report on the relationship between electrical properties of GaN-based MOS-HEMTs and experimental D_{it} distributions evaluated for the same structures. The N_2O-radical treatment is one of the effective processes for reducing the Al_2O_3/AlGaN interface states and improving the electrical properties of the GaN-based MOS-HEMTs.

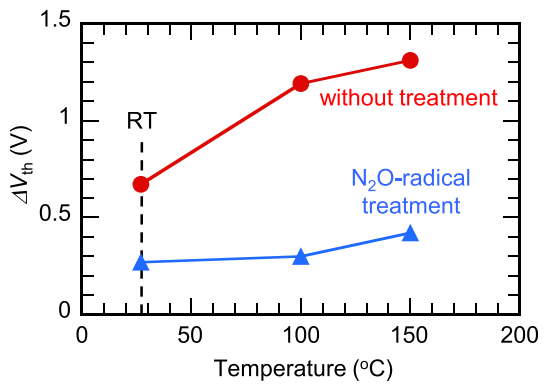

FIG. 12. Negative-gate-bias-induced V_{th} shifts of the MOS-HEMTs without and with the N_2O-radical treatment measured at RT, 100 °C, and 150 °C.

V. CONCLUSION

We have estimated the Al_2O_3/AlGaN interface state density distributions in the Al_2O_3/AlGaN/GaN MOS-HEMTs using the combination of the frequency dependent and photo-assisted C-V methods. The N_2O-radical treated MOS-HEMT showed smaller frequency dispersion of the C-V curves than that of the sample without the treatment, indicating the reduction of the interface states. The state densities were estimated to be 1×10^{12} cm^{-2} eV^{-1} or less around the midgap and 8×10^{12} cm^{-2} eV^{-1} near the conduction-band edge, which is approximately 40% less than those in the MOS-HEMT without treatment. We then investigated the impact of the reduced interface state densities on the electrical properties of the MOS-HEMTs. In the transfer curves, the decrease of transconductance was observed at high gate bias range where the parasitic channel is formed at the Al_2O_3/AlGaN interface. In this case, the N_2O-radical treated MOS-HEMT having the reduced interface states showed higher current density than that of the sample without treatment. We also have performed the negative-gate-bias-induced V_{th} instability measurements at RT to 150 °C. For the N_2O-radical treated MOS-HEMT, the reduced interface states led to more stable V_{th} even at high temperatures. The results indicated that the N_2O-radical treatment is effective both in reducing the Al_2O_3/AlGaN interface states and improving the electrical properties of the MOS-HEMTs. Control of the MOS interface states is one of the key technologies for improving operational performance and stability of the GaN-based devices.

ACKNOWLEDGMENTS

The authors would like to gratefully thank Dr. J. T. Asubar (Research Center for Integrated Quantum Electronics, Hokkaido University) for technical advice.

[1]U. K. Mishra, L. Shen, T. E. Kazior, and Y. F. Wu, Proc. IEEE **96**, 287 (2008).
[2]H. Kambayashi, Y. Satoh, S. Ootomo, T. Kokawa, T. Nomura, S. Kato, and T. P. Chow, Solid-State Electron. **54**, 660 (2010).
[3]M. Kanamura, T. Ohki, T. Kikkawa, K. Imanishi, T. Imada, A. Yamada, and N. Hara, IEEE Electron Device Lett. **31**, 189 (2010).

[4]J. Kashiwagi, T. Fujiwara, M. Akutsu, N. Ito, K. Chikamatsu, and K. Nakahara, IEEE Electron Device Lett. **34**, 1109 (2013).
[5]Z. Tang, Q. Jiang, Y. Lu, S. Huang, S. Yang, X. Tang, and K. J. Chen, IEEE Electron Device Lett. **34**, 1373 (2013).
[6]T. Hashizume, S. Ootomo, T. Inagaki, and H. Hasegawa, J. Vac. Sci. Technol. B **21**, 1828 (2003).
[7]T. Hashizume, S. Ootomo, and H. Hasegawa, Appl. Phys. Lett. **83**, 2952 (2003).
[8]D. Gregušová, R. Stoklas, K. Čičo, T. Lalinský, and P. Kordoš, Semicond. Sci. Technol. **22**, 947 (2007).
[9]E. Miyazaki, Y. Goda, S. Kishimoto, and T. Mizutani, Solid-State Electron. **62**, 152 (2011).
[10]J. Robertson and B. Falabretti, Mater. Sci. Eng. B **135**, 267 (2006).
[11]Y. Hori, C. Mizue, and T. Hashizume, Jpn. J. Appl. Phys., Part 1 **49**, 080201 (2010).
[12]X. Liu, R. Yeluri, J. Lu, and U. K. Mishra, J. Electron. Mater. **42**, 33 (2013).
[13]C. M. Jackson, A. R. Arehart, E. Cinkilic, B. McSkimming, J. S. Speck, and S. A. Ringel, J. Appl. Phys. **113**, 204505 (2013).
[14]C. Mizue, Y. Hori, M. Miczek, and T. Hashizume, Jpn. J. Appl. Phys., Part 1 **50**, 021001 (2011).
[15]S. Huang, S. Yang, J. Roberts, and K. J. Chen, Jpn. J. Appl. Phys., Part 1 **50**, 110202 (2011).
[16]Z. Yatabe, Y. Hori, S. Kim, and T. Hashizume, Appl. Phys. Express **6**, 016502 (2013).
[17]M. Ťapajna, M. Jurkovič, L. Válik, Š. Haščík, D. Gregušová, F. Brunner, E.-M. Cho, and J. Kuzmík, Appl. Phys. Lett. **102**, 243509 (2013).
[18]Y. Hori, C. Mizue, and T. Hashizume, Phys. Status Solidi C **9**(6), 1356 (2012).
[19]M. Miczek, C. Mizue, T. Hashizume, and B. Adamowicz, J. Appl. Phys. **103**, 104510 (2008).
[20]E. H. Nicollian and J. R. Brews, *MOS (Metal Oxide Semiconductor) Physics and Technology* (John Wiley & Sons, Inc., New Jersey, 2003), p. 325.
[21]M. Fagerlind, F. Allerstam, E. Ö. Sveinbjörnsson, N. Rorsman, A. Kakanakova-Georgieva, A. Lundskog, U. Forsberg, and E. Janzén, J. Appl. Phys. **108**, 014508 (2010).
[22]S. M. Sze and K. K. Ng, *Physics of Semiconductor Devices Third Edition* (John Wiley & Sons, Inc., New Jersey, 2007), p. 215.
[23]K. Ooyama, K. Sugawara, S. Okuzaki, H. Taketomi, H. Miyake, K. Hiramatsu, and T. Hashizume, Jpn. J. Appl. Phys., Part 1 **49**, 101001 (2010).
[24]A. Uedono, S. Ishibashi, S. Keller, C. Moe, P. Cantu, T. M. Katona, D. S. Kamber, Y. Wu, E. Letts, S. A. Newman, S. Nakamura, J. S. Speck, U. K. Mishra, S. P. DenBaars, T. Onuma, and S. F. Chichibu, J. Appl. Phys. **105**, 054501 (2009).
[25]F. González-Posada, J. A. Bardwell, S. Moisa, S. Haffouz, H. Tang, A. F. Braña, and E. Muñoz, Appl. Surf. Sci. **253**, 6185 (2007).
[26]M. Higashiwaki, S. Chowdhury, B. L. Swenson, and U. K. Mishra, Appl. Phys. Lett. **97**, 222104 (2010).
[27]B. Brennan, X. Qin, H. Dong, J. Kim, and R. M. Wallace, Appl. Phys. Lett. **101**, 211604 (2012).
[28]P. Sivasubramani, T. J. Park, B. E. Coss, A. Lucero, J. Huang, B. Brennan, Y. Cao, D. Jena, H. Xing, R. M. Wallace, and J. Kim, Phys. Status Solidi RRL **6**, 22 (2012).
[29]N. Shiozaki and T. Hashizume, J. Appl. Phys. **105**, 064912 (2009).
[30]C. Bae, G. B. Rayner, and G. Lucovsky, Appl. Surf. Sci. **216**, 119 (2003).
[31]M. Tajima, J. Kotani, and T. Hashizume, Jpn. J. Appl. Phys., Part 1 **48**, 020203 (2009).
[32]G. V. Soares, K. P. Bastos, R. P. Pezzi, L. Miotti, C. Driemeier, I. J. R. Baumvol, C. Hinkle, and G. Lucovsky, Appl. Phys. Lett. **84**, 4992 (2004).